PCCP

PAPER

View Article Online
View Journal | View Issue

Cite this: *Phys. Chem. Chem. Phys.*, 2017, **19**, 30914

Photoinduced dynamics in cycloparaphenylenes: planarization, electron–phonon coupling, localization and intra-ring migration of the electronic excitation†

N. Oldani,[a] S. K. Doorn,[b] S. Tretiak[b] and S. Fernandez-Alberti *[a]

Received 19th September 2017,
Accepted 6th November 2017

DOI: 10.1039/c7cp06426h

rsc.li/pccp

Cycloparaphenylenes represent the smallest possible fragments of armchair carbon nanotubes. Due to their cyclic and curved conjugation, these nanohoops own unique photophysical properties. Herein, the internal conversion processes of cycloparaphenylenes of sizes 9 through 16 are simulated using Non-Adiabatic Excited States Molecular Dynamics. In order to analyze effects of increased conformational disorder, simulations are done at both low temperature (10 K) and room temperature (300 K). We found the photoexcitation and subsequent electronic energy relaxation and redistribution lead to different structural and electronic signatures such as planarization of the chain, electron–phonon couplings, wavefunction localization, and intra-ring migration of excitons. During excited state dynamics on a picosecond time-scale, an electronic excitation becomes partially localized on a portion of the ring (about 3–5 phenyl rings), which is not a mere static contraction of the wavefunction. In a process of non-radiative relaxation involving non-adiabatic transitions, the latter exhibits significant dynamical mobility by sampling uniformly the entire molecular structure. Such randomized migration involving all phenyl rings, occurs in a wave-like fashion coupled to vibrational degrees of freedom. These results can be connected to unpolarized emission observed in single-molecule fluorescence experiments. Observed intra-ring energy transfer is subdued for lower temperatures and adiabatic dynamics involving low-energy photoexcitation to the first excited state. Overall our analysis provides a detailed description of photo excited dynamics in molecular systems with circular geometry, outlines size-dependent trends and connotes specific spectroscopic signatures appearing in time-resolved experimental probes.

I. Introduction

Cycloparaphenylenes ([*n*]CPPs, $n = 4,\ldots,18$) are well defined radially cyclic conjugated systems composed of *n* phenyl units linked at the *para* positions end-to-end[1] (see Fig. 1(a)). They represent interesting and unique molecular entities not only because of their aesthetic cyclic structures[2] but also because they constitute the smallest possible fragment of an armchair carbon nanotube.[3–7] Since their original attempts of synthesis,[8,9] CPPs moved from the merely academic interest to attractive targets for a large variety of applications in material science and technology such as photovoltaic, photoelectronic, and light-emission technologies. Their successful controlled synthesis and characterization has represented a challenge in the fields of synthesis chemistry,[2,10–18] computational material science[1,10,12,19–21] and fundamental physics.[22–25] They have served as triggers for the synthesis of a large variety of related nanohoops combining different units connected through different linkages[26–33] in an attempt to cross the bridge between small molecules and single-walled carbon nanotubes.[20,34–44]

CPPs constitute non-planar conjugated molecular systems in which the efficiency in π-orbital overlaps co-exists with bending strains introduced by the cyclic nanostructure.[45,46] Due to steric hindrances, dihedral angles between the phenyl rings in [*n*]CPPs are significant, being about 30 degrees.[37,47] For the even-numbered [*n*]CPPs, a high symmetry configuration with an alternating staggered arrangement of phenyl rings results for the lowest ground-state energy conformation.[1,34,48] Nevertheless, such a conformation is not possible for any odd-numbered [*n*]CPPs, leading to the presence of a "natural defect" in a frustrated structure typically localized to a few phenyls adopting more planar conformation.[49] The lack of chain end-effects, presence of structural frustration, and high symmetry furnish

[a] *Universidad Nacional de Quilmes, Roque Saenz Peña 352, B1876BXD Bernal, Argentina. E-mail: sfalberti@gmail.com*
[b] *Theoretical Division, Center for Nonlinear Studies (CNLS), and Center for Integrated Nanotechnologies (CINT), Los Alamos National Laboratory, Los Alamos, NM 87545, USA*

† Electronic supplementary information (ESI) available. See DOI: 10.1039/c7cp06426h

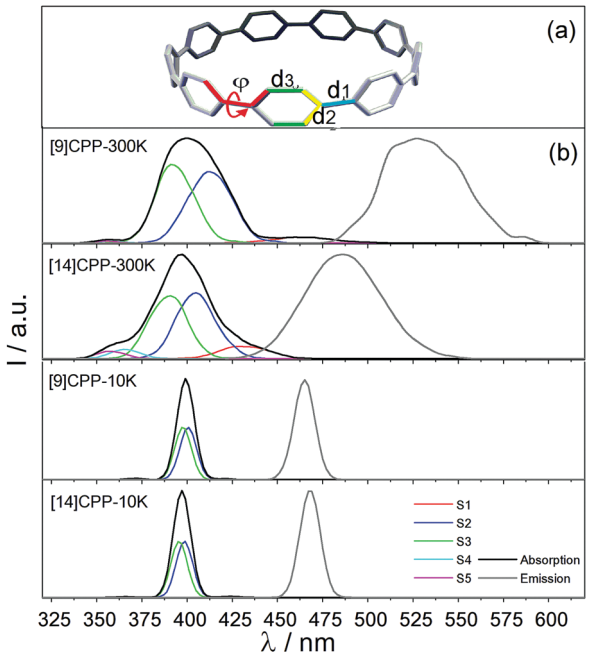

Fig. 1 (a) Schematic representation of [9]CPP ring indicating dihedral angle φ and bonds entering bond length alternation (BLA) parameter; (b) simulated absorption and emission spectra for [9]-, and [14]CPP at 300 K and 10 K with separated contributions of different excited states to the absorption spectrum.

[*n*]CPPs with unique linear and nonlinear optical properties as compared with linear conjugated molecules.[10,15–17,49] While the optical absorption maximum wavelength increases with the number of phenylene units in linear oligophenylenes, it is found to be independent of hoop size in [*n*]CPPs. Besides, CPPs were observed to be highly fluorescent, with an increasing red shift as [*n*]CPP hoop size decreases (as opposite to the trends observed in linear counterparts).[50] Moreover, the fluorescence quantum yield significantly increases with the size of the ring.[1,28,29,51] Due to these peculiar size-dependent optoelectronic properties,[52] they represent promising materials for implementation as organic semiconductors and sensors.

In order to achieve the desired control over optoelectronic properties, significant experimental and computational efforts have been devoted to studying the relationship between the molecular conformation and exciton delocalization in the excited states of cyclic π-conjugated molecules.[49,53] After photoexcitation, the intramolecular electronic and vibrational energy relaxation and redistribution lead to exciton localization on the subunits of the conjugated molecule,[54–59] introducing significant changes in the photophysical properties of the entire molecule.[49] For example, on one hand, excited-state dynamics can activate ultrafast torsional reorganization that planarizes and stabilizes the quinoidal structure of the excited state, resulting in an extension of the excitonic wave function.[60] On the other hand, an increase in hoop size induces conformational deformations and, hence, can facilitate the localization of the exciton on a part of the nanoring. This effect is expected to increase with temperature since disorder due to thermal fluctuations is expected to reduce the extent of exciton localization.

Non-adiabatic EXcited-States Molecular Dynamics (NEX-MD)[61,62] simulations provide detailed information on the correlation between torsional reorganization and exciton localization during the internal conversion process and subsequent relaxation on the lowest excited state. In a previous article,[49] we associate the efficient fluorescence in large [*n*]CPPs with a spatial localization of the exciton (self-trapping) due to strong vibronic coupling,[63] which breaks the Condon approximation and overrides the optical selection rules imposed by circular geometry. Herein, we extend our study of the internal conversion processes in [*n*]CPPs of different sizes in order to analyze the complex interplay between different structural and dynamics changes such as planarization of the chain, thermal fluctuations, bond length alternation with intramolecular redistribution of the electronic transition density expressed in terms of exciton localization, and intra-ring migration. The concomitance of these processes underlines the effects of strong electron–phonon couplings.

The paper is organized as follows. Section II provides a brief overview of the NEX-MD method, electronic transition densities calculation, excited-state normal mode calculation, and computational details. In Section III we present and discuss our results. Finally, Section IV summarizes our main findings and conclusions.

II. Methods

A. The NEX-MD methodology

The NEX-MD[61,62] is an efficient and sufficiently accurate method developed to simulate photoinduced dynamics of large organic conjugated molecules involving multiple coupled electronic excited states. It combines the fewest switches surface hopping (FSSH) algorithm[64,65] with "on the fly" analytical calculations of excited-state energies,[66–68] gradients,[69,70] and non-adiabatic coupling terms.[61,71–73] For this purpose, correlated excited states are calculated using the collective electron oscillator (CEO) approach[74–76] with the configuration interaction singles (CIS) formalism implemented with the semiempirical AM1 Hamiltonian.[77] This level of approximation has been successfully applied to many molecular systems, including conjugated materials[78–83] and provides an adequate description of excitonic states and excited state dynamics in [*n*]CPPs.[49]

In FSSH formalism, the probabilities of quantum transitions between excited states are prescribed by non-adiabatic coupling vectors (NACR), which are also calculated analytically.[61] These quantities are defined as

$$\mathbf{d}_{\alpha\beta} = \langle \phi_\alpha(\boldsymbol{r}; \boldsymbol{R}(t)) | \nabla_{\boldsymbol{R}} \phi_\beta(\boldsymbol{r}; \boldsymbol{R}(t)) \rangle \quad (1)$$

where $\boldsymbol{r}$ and $\boldsymbol{R}(t)$ are the electronic and nuclear vector coordinates, respectively, and $\phi_\alpha(\boldsymbol{r}; \boldsymbol{R}(t))$ is the αth electronic state wavefunction. The directions of NACR represent the non-adiabatic contribution to the direction of the main driving force on the nuclei during electronic transitions.[84] Further details of the NEX-MD approach, implementation,

advantages and testing parameters can be found in our previous work.[61,62,85]

B. Transient (de)localization of the electronic transition density

During NEX-MD simulations, the intramolecular electronic energy redistribution is followed using the time-dependent localization of the electronic transition density for the current state. The CEO approach[78,86] calculates transition density matrices $(\rho^{g\alpha})_{nm} \equiv \langle \phi_\alpha(\boldsymbol{r};\boldsymbol{R}(t))|c_m^+ c_n|\phi_g(\boldsymbol{r};\boldsymbol{R}(t))\rangle$ (denoted electronic normal modes) using the ground-state density matrix, where the subindex g refers to the ground state. Here $c_m^+(c_n)$ represents the creation (annihilation) electronic operator; and indices n and m refer to atomic orbital (AO) basis functions. The diagonal elements of $(\rho^{g\alpha})_{nn}$ represent the changes in the electronic density induced by photoexcitation from the ground state g to an excited electronic α state.[87] According to the normalization condition $\sum_{n,m}\left(\rho_{nm}^{g\alpha}(t)\right)^2 = 1$ fulfilled within the CIS approximation[68] the transition density localized on each phenyl unit i at each time of the NEX-MD simulations can be written as:

$$\left(\rho_{\mathrm{phe},i}^{g\alpha}(t)\right)^2 = \sum_{n_\mathrm{A} m_\mathrm{A}} \left(\rho_{n_\mathrm{A} m_\mathrm{A}}^{g\alpha}(t)\right)^2 \quad (2)$$

where the index A runs over all atoms localized in the corresponding phenyl unit. In order to measure the extent of (de)localization of the excitation among the phenyl units of an [n]CPP, we define the phenyl-unit participation number[88,89] as

$$P_\mathrm{ring}(t) = \left[\sum_i^n \left(\rho_{\mathrm{phe},i}^{g\alpha}(t)\right)^4\right]^{-1} \quad (3)$$

Values of $P_\mathrm{ring}(t) \approx 1$ indicate a complete localization of the transition density to a single phenyl unit, while values of $P_\mathrm{ring}(t) \approx n$ correspond to transition densities fully delocalized accross the n phenyl units.

C. Exciton intra-ring migration

The dynamical aspects of the exciton intra-ring self-trapping have been analyzed using the following procedure:

(1) $P_\mathrm{ring}(t_0)$ is evaluated at t_0.

(2) The n phenyl units of [n]CPP are sorted by decreasing contribution to the electronic transition density $\rho^{g\alpha}(t_0)$.

(3) A vector $v(t_0)$ is constructed, where the elements $v_i(t_0)$, associated to each phenyl unit, are

$$= 1 \text{ if } s_i < P_\mathrm{ring}(t_0)$$

$$= 0 \text{ otherwise}$$

Here s_i is the rank of the ith element according to 2.

(4) Steps 1 to 3 are repeated throughout the simulation at every time-step t.

The resulted ith element of vector $v(t)$, averaged over the entire ensemble of trajectories, represents the probability of the ith phenyl ring to retain a significant contribution to $\rho^{g\alpha}(t)$. This quantifies participation of every phenyl ring in the electronic dynamics following photoexcitation, thus allowing to track the intra-ring migration of the excited state wavefunction.

D. Excited-state equilibrium normal mode analysis

Excited-state equilibrium normal modes (ES-ENM(S_1)) analysis has been performed at the equilibrium $\boldsymbol{R}_0$ structure obtained by previously performing geometry optimization of the molecular system at the lowest excited-state S_1. Geometry optimization was performed on the [n]CPPs with the AM1 semi-empirical Hamiltonian, using Gaussian 09.[90]

ES-ENM(S_1) were computed from the mass-weighted Hessian matrix $\mathbf{H}$ with elements

$$H_{ij}(\boldsymbol{R}_0) = -\partial^2 E_1/\partial q_i \partial q_j|_{\boldsymbol{R}_0} \quad (4)$$

where E_1 is the potential energy of S_1 state and $q_i = \sqrt{m_i}\left(\boldsymbol{R}_i - \boldsymbol{R}_{0,i}\right)$ is mass weighted Cartesian displacement of the ith atom with mass m_i and Cartesian coordinates $\boldsymbol{R}_{0,i}(X_{0,i},Y_{0,i},Z_{0,i})$ defined in a body-fixed reference frame with the origin at the center of mass of the molecule and axes corresponding to its principle axes of inertia. Upon diagonalization of $\mathbf{H}$, the set of orthonormal ES-ENM(S_1) are defined by the set of eigenvectors with frequencies $\nu_\alpha = \sqrt{\lambda_\alpha}/2\pi$, where $\lambda_\alpha (i = 1, \ldots, 3N-6)$ are the eigenvalues of $\mathbf{H}$. More details about the calculations of ES-ENM(S_1) can be found elsewhere.[91]

E. Computational details

The NEX-MD simulations were conducted on [n]CPPs with n = 9, 12, 14, 15, and 16. Both room (300 K) and low (10 K) temperatures were considered. For each temperature, equilibrated ground state (S_0) molecular dynamics simulations were performed up to 1 ns. Here a Langevin thermostat with a friction coefficient of 20 ps^{-1} was employed. Each trajectory provided 400 snapshots sampling ground state conformational space (nuclei initial positions and momenta) for the subsequent NEX-MD simulations. The initial excited state is populated according to a Frank–Condon window given by $g_\alpha(\boldsymbol{r},\boldsymbol{R}) = \exp[-T^2(E_\mathrm{laser} - \Omega_\alpha)^2]$ where E_laser, expressed in units of fs^{-1} as well as Ω_α, represents the energy of a laser centred at $\sim$400 nm that corresponds to the maximum of the absorption spectrum. A Gaussian laser pulse, $f(t) = \exp(-t^2/2T^2)$, with T^2 = 42.5 fs corresponding to a FWHM (Full Width at Half Maximum) of 100 fs has been used. For each NEX-MD trajectory, the relative values of $g_\alpha(\boldsymbol{r},\boldsymbol{R})$ weighted by the oscillator strengths of each state α have been used to select its initial excited state.

Ten electronic states and their corresponding non-adiabatic couplings were included in the simulations. 400 NEX-MD trajectories of 500 fs duration at 300 K (room temperature) and 2 ps duration at 10 K were propagated in order to obtain reasonable statistics. A classical time step of 0.5 fs (0.1 fs) has been used for nuclei propagation in ground-state and NEX-MD simulations respectively. Besides, a quantum time step of 0.025 fs has been used to propagate the electronic degrees of freedom during the NEX-MD simulations. In order to identify and

deal with trivial unavoided crossings, the quantum time step was further reduced by a factor of 40 in the vicinity of such crossings.[92]

In addition, we have calculated 400 trajectories of 500 fs duration at 300 K (room temperature) and 2 ps duration at 10 K but for excited state adiabatic dynamics at the first excited state S_1. Here an original ensemble has been excited to S_1 and no quantum transitions were allowed during propagation. This provides direct comparison data *vs.* respective non-adiabatic simulations where additional electronic energy is converted to heat during internal conversion.

III. Results and discussion

CPPs are nanohoops composed of n phenyl units. For example, [9]CPP structure is drawn in Fig. 1(a). Fig. 1(b) shows the calculated absorption and emission spectra for [9]-, and [14]CPP molecules computed at 300 K and 10 K. These quantities for other molecules are given in ESI† (Fig. S1). The spectra are calculated as superposition of absorptions and emissions of individual molecules across an entire ensemble. Here absorptions are relevant to a collection of the snapshots from ground state trajectory as described above, whereas emissions were computed for the same ensemble but snapshots taken at the end of trajectories for the adiabatic dynamics of the first excited state S_1. As seen in Fig. 1(b), conformational disorder due to thermal fluctuation leads to natural broadening, albeit Frank–Condon effects are missing from such consideration. In agreement with previous experimental and theoretical works[1,34,49] the absorption maxima wavelengths were found to be almost independent of the hoop size. In contrast, the emission spectra manifest an increasing red shift with decrease of [*n*]CPP hoop size.

The main absorption peaks are dominated by roughly equivalent contributions of both S_2 and S_3 excited states, that are strongly optically allowed due to the selection rules for circular geometry.[49] At optimal geometry, S_2 and S_3 states are degenerate, which is lifted at the finite temperature. As previously discussed,[49] the independence of the absorption maxima on the molecular size is a consequence of a mutual cancelation of two main effects that take place while increasing the size of the CPP molecule and reducing the backbone strain: an increase in the conjugation length (red shift) and an increase of the torsions between phenyl units (blue shift). The S_1 state is optically forbidden in circular geometries due to symmetry.[49] Nevertheless, thermal fluctuations introduce perturbations in the electronic wave function, which result in small but nonzero oscillator strength and appearance of the minor absorption shoulder in the red at high temperature.

Fig. 2 shows the distribution of the dihedral angles between neighboring phenyls for [9]-, and [14]CPP molecules in the ground-state at 300 K and 10 K across the conformational ensemble. These quantities for other molecules are given in ESI† (Fig. S2). In agreement with previous studies,[10,12,19] we observe an increase of the average values of dihedral angles with the size of the hoop. The large conformational disorder induced at high

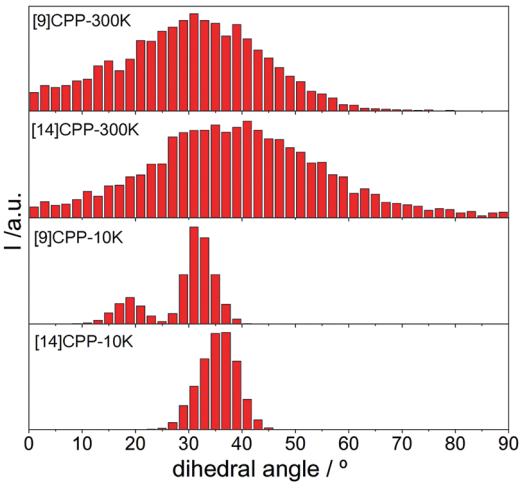

Fig. 2 Dihedral angle distributions at the initial ground state configurations at 300 K and 10 K for [9]- and, [14]CPPs.

temperature (300 K) leads to wide dihedral angle distributions with a single maximum at about 30–40°. As expected, this distribution for [14]CPP at low temperature (10 K) just gets narrower. In contrast, the dihedral angle distribution of [9]CPP at 10 K features an additional peak evidencing presence of localized frustrated structures[49] where one of the rings is connected to its neighbors by dihedral angles of about 15–20°.

The internal conversion processes driven by non-radiative relaxation of [*n*]CPPs with n = 9, 12, 14, 15, and 16 was further studied using the NEX-MD simulations. To analyze photoexcitation dynamics of [*n*]CPPs, we start with the evolution in time of the average population on S_1 obtained from the accumulated fraction of NEX-MD trajectories arriving to this state at each time as shown in Fig. 3. As expected, we observe a fast increase

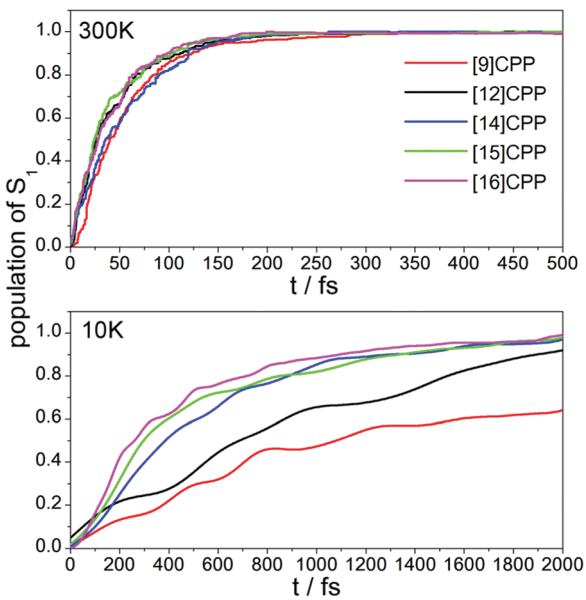

Fig. 3 Time dependence of the average population on S_1 state for all CPP molecules studied obtained from the accumulated fraction of NEX-MD trajectories in that state at each time.

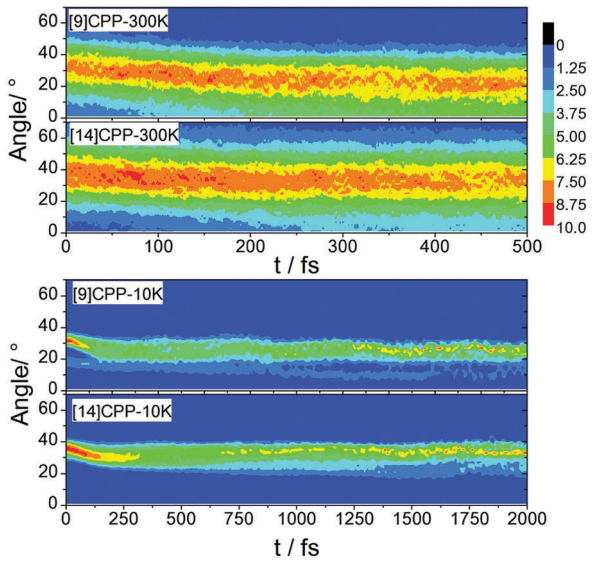

Fig. 4 Time evolution of dihedral angle distribution during the NEX-MD simulations at 300 K and 10 K for [9]- and [14]CPPs.

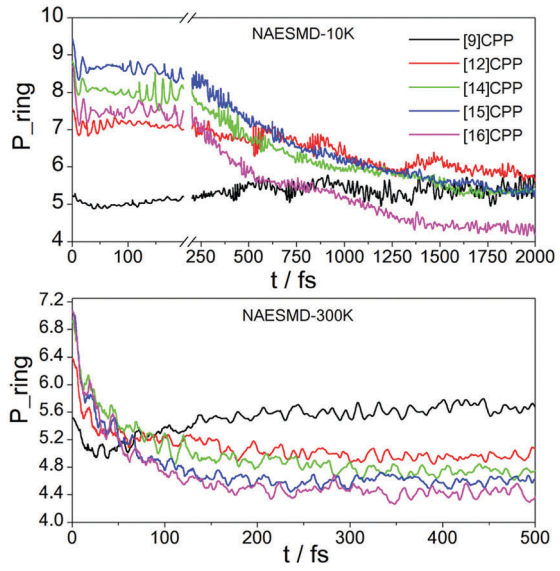

Fig. 5 Time dependence of the participation number $P_{ring}(t)$ for NEX-MD simulations of CPP molecules studied at 300 K and 10 K.

in the S_1 population with time. At high temperature, the process seems to be weakly dependent on the hoop size, and at about 200 fs all photoexcited trajectories end up on the S_1 state. In contrast, the process is substantially slower at low temperature, where the relaxation rate noticeably decreases with the hoop size. In part, this is explained with the larger effective gap between S_1 and S_2/S_3 states in the smaller rings in the absence of thermal fluctuation, which reduces the value of non-adiabatic coupling and thus the rate of quantum transitions.

In order to relate this behavior to nuclear motions in the excited states, dihedral angles between neighboring phenyls have been analyzed throughout the NEX-MD simulations. Fig. 4 summarizes these data in a form of two-dimensional plots. These plots for other molecules are given in ESI† (Fig. S3). In fact, Fig. 1 represents the respective slices of this plot at $t = 0$. Previous experimental and theoretical works reported as a general phenomenon that π–π* electronic excitations in conjugated molecules frequently lead to more planar conformations.[60,82,93–95] Furthermore, observed ring planarization in the excited state of these molecules is directly relevant to the well-known planarization of biphenyls, for example reported in ref. 96.

As can be seen in Fig. 4, this effect is observed in [*n*]CPPs as well. As it has been previously pointed out,[10] planarization in the excited states leads to larger Stokes shifts in smaller CPPs as a result of larger degrees of structural relaxation in the S_1 state. The enhanced curvature in smaller CPPs leads to greater sp^3 hybridization with lobes oriented inside the nanohoops, reducing steric effects that hinder planarization. This effect is more evident at higher temperature, where the torsion angle distributions become wider due to conformational disorder. Subsequently, this effect lowers the center of distribution in small CPPs (*e.g.*, in [9]CPP), and appears mostly as a shoulder in the distribution around 10–20 degrees in large CPPs (*e.g.*, in [14]CPP). Similar trends are observed for lower temperature, however with narrower angle distribution.

Observed planarization and localization are the characteristic signatures of the exciton self-trapping in the excited state dynamics leading to efficient fluorescence from S_1 state in large CPP hoops.[49] The participation number, $P_{ring}(t)$ (see Section 2B) provides a convenient and quantitative measure of the spatial excitation extent in [*n*]CPP. Fig. 5 displays the evolution of $P_{ring}(t)$ throughout the NEX-MD for the CPP family at both high and low temperature. $P_{ring}(t)$ is always lower than n due to a non-uniform distribution of the exciton density on the ring itself as well as structural disorder introduced by thermal fluctuations. The effect is expected to be more pronounced at high temperature. Indeed, even in the ground state geometries at higher temperature, the photoexcitation initially spreads effectively only over 7 rings in all systems except [9]CPP (5.5 rings). $P_{ring}(t)$ then reduces to about 5 except for [9]CPP, where the size reduces first and then slowly returns to the nearly original value. For [12]-, [14]-, and [15]CPP, higher values of $P_{ring}(t)$ can be observed during all the NEX-MD at low temperature with respect to the corresponding values at high temperature. These behaviors reflect a complex interplay of conformational disorder induced by temperature, planarization of the structure induced by excited state dynamics and structural strain increasing in smaller rings.

In order to analyze the dynamic aspects of the exciton intra-ring self-trapping, the probability of each phenyl ring to retain a significant contribution to $\rho^{gg}(t)$ has been calculated following the procedure described in Section 2C. Fig. 6 summarizes the obtained results for [9]CPP (see also a movie showing the exciton redistribution in a NEX-MD for [9]CPP at ESI†). Our corresponding results for other molecules are given in ESI† (Fig. S4 and S5). The internal conversion process leads to a final similar probability for all phenyl rings of the nanohoop (panel a). That is, the exciton localization during the internal conversion process is not merely a static contraction of the electronic

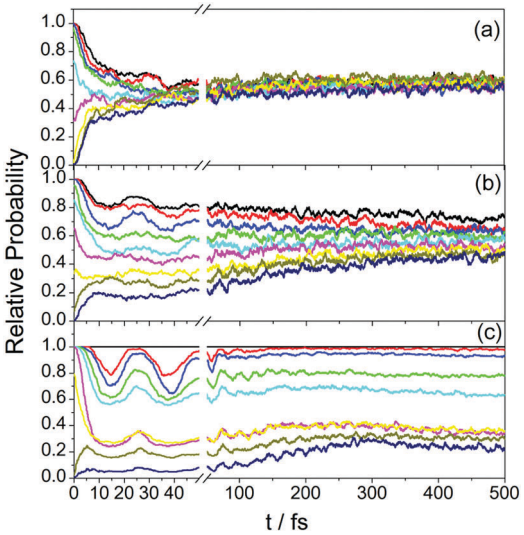

Fig. 6 Variation in time of the relative probability of each phenyl ring to retain a significant contribution to total electronic transition density for [9]CPP calculated during (a) NEX-MD simulations at 300 K; (b) adiabatic molecular dynamics on S_1 state at 300 K; (c) adiabatic molecular dynamics on S_1 state at 10 K.

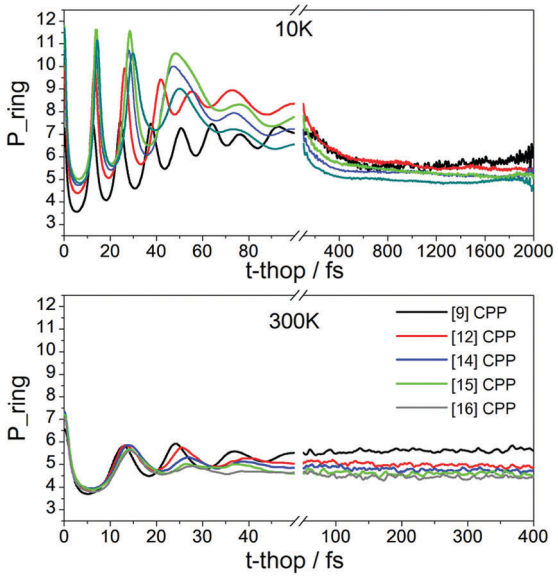

Fig. 7 Average participation number $P_{ring}(t)$ during the NEX-MD simulations of all CPP molecules studied at 10 K and 300 K as a function of delay time relative to the moment of non-adiabatic $S_2 \rightarrow S_1$ transition.

wavefunction to a specific spot on the ring such as a structural defect. Instead, the exciton experiences an intra-ring migration uniformly involving all phenyl rings. Previous single-molecule fluorescence experiments performed on π-conjugated spoked-wheel macrocycles have revealed random exciton localization.[97,98] That is, the spatial localization of excitation energy caused by nuclear rearrangements during electronic relaxation does not seem to follow a unique pathway. On the contrary, the exciton localization in π-conjugated nanorings has been revealed as a non-deterministic process that arises randomly on different units.

It is interesting at this point to analyse if the final random exciton self-trapping is a consequence of the non-adiabatic electronic energy transfer during the internal conversion process or if it is a consequence of intrinsic vibrational fluctuations on the S_1 state. For this purpose, adiabatic molecular dynamics have been performed by initially exciting the molecular system on the S_1 state. The results are shown in Fig. 6(b). We can observe that thermally induced fluctuations and vibrations on the S_1 state are also responsible for the final random distribution of $\rho^{g\alpha}(t)$ among all phenyl rings of the nanohoop. Nevertheless, the process seems to be much less effective than the one observed during NEX-MD simulations. A drastic reduction of thermally induced fluctuations and vibrations at 10 K leads to temporary stable, virtually 'unmovable' excitation. This is shown in Fig. 6(c) where results corresponding to adiabatic molecular dynamics simulations on the S_1 state are displayed. Thus, motion of the excitation on the ring is strongly correlated with an amount of available vibrational energy due to thermal fluctuations or non-equilibrium relaxation of excited states.

We next analyze the relationships between excitonic delocalization and transfer of electronic energy into vibrations upon non-adiabatic transitions to the lowest excited state S_1. Fig. 7 shows the average values of $P_{ring}(t)$ as a function of delay time, relative to the moment of hop from S_2 to S_1 potential energy surface, when the nuclear motion activates due to access of electronic energy deposited to vibrations in the direction of non-adiabatic coupling vector. After this transition, we observe $P_{ring}(t)$ oscillations during the first ~100 fs both at high and low temperature. These fluctuations in the localization/delocalization of the exciton on S_1 surface occur with a period of roughly 13 fs, which is directly relevant to C–C stretching motion of the phenyl ring initiated by quantum transitions. The fact that these oscillations appear for the ensemble average for both temperatures (albeit, they are subdued as expected for the room temperature), suggests the possibility of formation of 'coherent phonons' of the C–C stretching mode, when all molecules vibrate in-phase on the ultrafast timescales, coherently evolving with the electronic system. Such phenomena were previously observed in other materials such as carbon nanotubes.[99–101]

The dynamical features contributing to these fluctuations are controlled by the non-adiabatic coupling vector, which dictates the initial intramolecular electronic and vibrational energy redistribution that takes place after the $S_2 \rightarrow S_1$ transition.[102,103] Its projection on the basis of ES-ENM(S_1) reveals main contributions of 221st and 222nd ENMs with frequencies of 1766.7 cm^{-1} and 1776.7 cm^{-1} respectively. These modes are displayed in Fig. 8(a). They correspond to equivalent motions associated to in-plane E_{2g} vibrations of benzene but involving different phenyl units on the ring.

Molecular conformations during S_1 excited-state dynamics can be analysed by following the bond length alternation (BLA). BLA reflects the inhomogeneity in the distribution of electrons along the π-conjugated molecule and it is generally defined as a

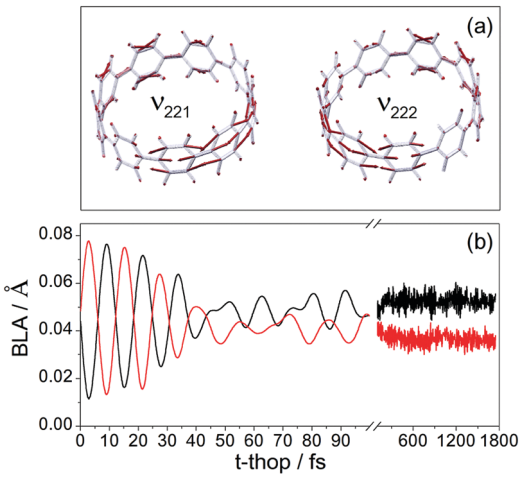

Fig. 8 (a) ES-ENM(S_1) that overlap the most with the non-adiabatic coupling vector at the moment of non-adiabatic $S_2 \rightarrow S_1$ transition; (b) BLA for each half of the nanohoop as a function of the delay time for a typical NEX-MD simulation of [9]CPP at 10 K.

difference between single and double bond lengths along the cycle chain

$$\mathrm{BLA} = d_1 - d_2 \cdot \frac{2}{3} - d_3 \cdot \frac{1}{3} \qquad (5)$$

where d_1, d_2, and d_3 are indicated in Fig. 1(a). Smaller values of BLA are associated with better π-conjugation between neighboring phenyl rings and, therefore, an enhancement of the electronic delocalization.[53,95,104] The nanoring may be partitioned in two equivalent halves following maximum amplitudes in the participating vibrational normal modes as shown in Fig. 8(a). As a result, Fig. 8(b) shows BLA for each half of [9]CPP as a function of delay time. We observe the out-of-phase oscillations in the values of BLA for each half of the molecule. This behaviour is a consequence of the out-of-phase motion between different blocks of phenyl units observed in the associated 221st and 222nd vibrational modes. That is, non-adiabatic $S_2 \rightarrow S_1$ electronic energy transfer introduces vibronic coupling that ensures a concomitant intramolecular vibrational energy flow into specific vibrational modes. As a result, fluctuations of either $\rho^{g\alpha}(t)$ localization and geometrical features are observed during the earlier times after the $S_2 \rightarrow S_1$ transition, leading to a final random exciton localization at longer times.

IV. Conclusions

Cyclic conjugated molecules represent a new class of functional chromophores with unique geometry, conformations and optoelectronic properties, with photophysical behaviours that are determined in distinctly different ways than those typical of the selection rules of linear oligomers. Understanding photoexcitation dynamics in such systems is a requisite for all applications. In this study we model non-adiabatic electron-vibrational dynamics and non-radiative relaxation following optical excitation in cycloparaphenylene molecular family, [n]CPPs with n = 9, 12, 14, 15, and 16 at high (300 K) and low (10 K) temperatures. After populating optically allowed quasi-degenerate S_2/S_3 states, we find that the internal conversion process leads to efficient population decay to the lowest S_1 excited state. While at high temperature the process seems to be independent on the hoop size, at low temperature it occurs faster with an increasing hoop size, partially owing to the reduced gap between S_2/S_3 and S_1 states. This behavior can also be related to nuclear motion/vibrational normal modes in the excited states leading to reduced bond length alternation and local planarization of the chain upon relaxation. During our simulations, such photoinduced planarization is more efficient in small CPPs than that in large rings due to increased structural strain. This effectively reduces the vibronic couplings in small systems during the internal conversion at low temperature, however, the large conformational disorder due to high temperature fluctuations seems to overcome it.

Observed conformational changes drive the wavefunction localization and ultimately exciton self-trapping during the internal conversion process in all hoops considered. While the effectiveness in the localization of the excitation increases with the temperature for [12]–[16]CPPs, this is not the case for [9]CPP, for which the final extent of localization seems to be independent of the temperature. This is a consequence of a competition between order and disorder that takes place during the internal conversion. Ordering is introduced by an efficient overlap between π-orbitals of neighboring phenyl rings, and disorder is the result of steric hindrance between phenyl units. While the former prevails in the small [9]CPP, the latter dominates the dynamics in the larger rings due to weakening of the overall structural strain.

Our analysis quantitatively demonstrates that internal conversion of CPPs leads to the final similarity in probabilities for each phenyl ring to retain a significant contribution to the electronic transition density irrespectively on the initial excitation. This finding underpins unpolarized emission observed in such systems in single-molecule fluorescence experiments.[105] We observe that the exciton localization is not merely a static contraction of the electronic wavefunction. The exciton actually experiences a randomized intra-ring migration involving all phenyl rings. This behaviour results from both non-adiabatic electronic energy transfer and thermally induced vibrational motions on the final S_1 state. Subsequent to the $S_2/S_3 \rightarrow S_1$ relaxation, fluctuations in the localization and delocalization of the wavefunction indicate an effective direct flow of electronic energy into specific vibrational modes of the S_1 state.

Conflicts of interest

There are no conflicts to declare.

Acknowledgements

N. O. and S. F. A. are supported by CONICET, UNQ, ANPCyT (PICT- 2014-2662). S. T. and S. K. D. acknowledges support from Los Alamos National Laboratory (LANL) Directed Research and

Development Funds. LANL is operated by Los Alamos National Security, LLC, for the National Nuclear Security Administration of the U.S. Department of Energy under contract DE-AC52-06NA25396. This work was performed in part at the Center for Integrated Nanotechnology (CINT), a U.S. Department of Energy, Office of Basic Energy Sciences user facility. We also acknowledge the LANL Institutional Computing (IC) Program for providing computational resources.

References

1 Y. Segawa, A. Fukazawa, S. Matsuura, H. Omachi, S. Yamaguchi and S. Irle, *et al.*, Combined experimental and theoretical studies on the photophysical properties of cycloparaphenylenes, *Org. Biomol. Chem.*, 2012, **10**, 5979–5984.
2 Y. Segawa, S. Miyamoto, H. Omachi, S. Matsuura, P. Senel and T. Sasamori, *et al.*, Concise synthesis and crystal structure of [12]CPP, *Angew. Chem., Int. Ed.*, 2011, **50**, 3244.
3 M. Iyoda, J. Yamakawa and M. J. Rahman, Conjugated Macrocycles: Concepts and Applications, *Angew. Chem., Int. Ed.*, 2011, **50**, 10522.
4 T. Kawase and H. Kurata, Ball-, Bowl-, and Belt-Shaped Conjugated Systems and Their Complexing Abilities: Exploration of the Concave–Convex π–π Interaction, *Chem. Rev.*, 2006, **106**, 5250.
5 B. Steinberg and L. Scott, New Strategies for Synthesizing Short Sections of Carbon Nanotubes, *Angew. Chem., Int. Ed.*, 2009, **48**, 5400.
6 G. Bodwell, Carbon nanotubes: growth potential, *Nat. Nanotechnol.*, 2010, **5**, 103.
7 R. Jasti and C. Bertozzi, Progress and challenges for the bottom-up synthesis of carbon nanotubes with discrete chirality, *Chem. Phys. Lett.*, 2010, **494**, 1.
8 V. Parekh and P. Guha, Synthesis of *p*,*p*′-diphenylene disulfide, *J. Indian Chem. Soc.*, 1934, **11**, 95.
9 R. Friederich, M. Nieger and F. Vögtle, Auf dem Weg zu makrocyclischen *para*-Phenylenen, *Chem. Ber.*, 1993, **126**, 1723.
10 R. Jasti, J. Bhattacharjee, J. Neaton and C. Bertozzi, Synthesis, Characterization, and Theory of [9]-, [12]-, and [18]Cycloparaphenylene: Carbon Nanohoop Structures, *J. Am. Chem. Soc.*, 2008, **130**, 17646–17647.
11 H. Takaba, H. Omachi, Y. Yamamoto, J. Bouffard and K. Itami, Selective Synthesis of [12]Cycloparaphenylene, *Angew. Chem., Int. Ed.*, 2009, **48**, 6112.
12 Y. Segawa, H. Omachi and K. Itami, Theoretical Studies on the Structures and Strain Energies of Cycloparaphenylenes, *Org. Lett.*, 2010, **12**, 2262.
13 H. Omachi, S. Matsuura, Y. Segawa and K. Itami, Modular and Size-Selective Synthesis of [*n*]Cycloparaphenylenes: A Step toward the Selective Synthesis of [*n*,*n*] Single-Walled Carbon Nanotubes, *Angew. Chem., Int. Ed.*, 2010, **49**, 10202.
14 Y. Segawa, P. Šenel, S. Matsuura, H. Omachi and K. Itami, [9]Cycloparaphenylene: Nickel-mediated Synthesis and Crystal Structure, *Chem. Lett.*, 2011, **40**, 423.
15 S. Yamago, Y. Watanabe and T. Iwamoto, Synthesis of [8]Cycloparaphenylene from a Square-Shaped Tetranuclear Platinum Complex, *Angew. Chem., Int. Ed.*, 2010, **49**, 757.
16 T. Iwamoto, Y. Watanabe, Y.-I. Sakamoto, T. Suzuki and S. Yamago, Selective and Random Syntheses of [*n*]Cycloparaphenylenes (*n* = 8–13) and Size Dependence of Their Electronic Properties, *J. Am. Chem. Soc.*, 2011, **133**, 8354.
17 T. Sisto, M. Golder, E. Hirst and R. Jasti, Selective Synthesis of Strained [7]Cycloparaphenylene: An Orange-Emitting Fluorophore, *J. Am. Chem. Soc.*, 2011, **133**, 15800.
18 H. Kim, H. J. Lee and D. P. Kim, Flow-Assisted Synthesis of [10]Cycloparaphenylene through Serial Microreactions under Mild Conditions, *Angew. Chem., Int. Ed.*, 2016, **55**(4), 1422–1426.
19 D. Sundholm, S. Taubert and F. Pinchierri, Calculation of absorption and emission spectra of [*n*]cycloparaphenylenes: the reason for the large Stokes shift, *Phys. Chem. Chem. Phys.*, 2010, **12**, 2751–2757.
20 B. Wong, Optoelectronic Properties of Carbon Nanorings: Excitonic Effects from Time-Dependent Density Functional Theory, *J. Phys. Chem. C*, 2009, **113**, 21921–21927.
21 C. Camacho, T. Niehaus, K. Itami and S. Irle, Origin of the size-dependent fluorescence blueshift in [*n*]cycloparaphenylenes, *Chem. Sci.*, 2013, **4**, 187–195.
22 P. Evans and R. Jasti, Molecular Belts, *Top. Curr. Chem.*, 2014, **349**, 249–290.
23 H. Chen, M. Golder, F. Wang, R. Jasti and A. Swan, Raman spectroscopy of carbon nanohoops, *Carbon*, 2013, **67**, 203–213.
24 A. Zabula, A. Filatov, J. Xia, R. Jasti and M. Petrukhina, Tightening of the Nanobelt upon Multielectron Reduction, *Angew. Chem., Int. Ed.*, 2013, **52**, 5033–5036.
25 M. R. Talipov, R. Jasti and R. Rathore, A Circle Has No End: Role of Cyclic Topology and Accompanying Structural Reorganization on the Hole Distribution in Cyclic and Linear Poly-p-phenylene Molecular Wires, *J. Am. Chem. Soc.*, 2015, **137**(47), 14999–15006.
26 H. Omachi, T. Nakayama, E. Takahashi, Y. Segawa and K. Itami, Initiation of carbon nanotube growth by well-defined carbon nanorings, *Nat. Chem.*, 2013, **5**, 572–576.
27 E. Hirst, F. Wang and J. Jasti, Theoretical Analysis of [5.7]*n*Cyclacenes: Closed-Shell Cyclacene Isomers, *Org. Lett.*, 2011, **13**, 6220–6223.
28 P. Li, T. Sisto, E. Darzi and R. Jasti, The Effects of Cyclic Conjugation and Bending on the Optoelectronic Properties of Paraphenylenes, *Org. Lett.*, 2013, **16**, 182–185.
29 M. Fujitsuka, D. Cho, T. Iwamoto, S. Yamago and T. Majima, Size-dependent fluorescence properties of [*n*]cycloparaphenylenes (*n* = 8–13), hoop-shaped π-conjugated molecules, *Phys. Chem. Chem. Phys.*, 2012, **14**, 14585–14588.
30 M. Golder, B. Wong and R. Jasti, Photophysical and theoretical investigations of the [8]cycloparaphenylene radical cation and its charge-resonance dimer, *Chem. Sci.*, 2013, **4**, 4285–4291.
31 S. M. Bachrach and Z. C. Zayat, ''Planetary Orbit'' Systems Composed of Cycloparaphenylenes, *J. Org. Chem.*, 2016, **81**(11), 4559–4565.

32 B. N. Taber, C. F. Gervasi, J. M. Mills, D. A. Kislitsyn, E. R. Darzi and W. G. Crowley, *et al.*, Quantum Confinement of Surface Electrons by Molecular Nanohoop Corrals, *J. Phys. Chem. Lett.*, 2016, **7**(16), 3073–3077.

33 G. Povie, Y. Segawa, T. Nishihara1, Y. Miyauchi and K. Itami, Synthesis of a carbon nanobelt, *Science*, 2017, **356**(6334), 172–175.

34 S. Lewis, Cycloparaphenylenes and related nanohoops, *Chem. Soc. Rev.*, 2015, **44**, 2221–2304.

35 S. Kammermeier and R. Herges, Picotubes, *Angew. Chem., Int. Ed. Engl.*, 1996, **35**, 417.

36 M. Machón, S. Reich, J. Maultzsch, H. Okudera, A. Simon and R. Herges, *et al.*, Structural, electronic, and vibrational properties of (4,4) picotube crystals, *Phys. Rev. B: Condens. Matter Mater. Phys.*, 2005, **72**, 155402.

37 A. Goller and U. Grummt, Torsional barriers in biphenyl, 2,2′-bipyridine and 2-phenylpyridine, *Chem. Phys. Lett.*, 2000, **321**, 399.

38 R. Herges, Topology in Chemistry: Designing Möbius Molecules, *Chem. Rev.*, 2006, **106**, 4820.

39 H. Omachi, Y. Segawa and K. Itami, Synthesis and Racemization Process of Chiral Carbon Nanorings: A Step toward the Chemical Synthesis of Chiral Carbon Nanotubes, *Org. Lett.*, 2011, **13**, 2480.

40 S. Hitosugi, W. Nakanishi, T. Yamasaki and H. Isobe, Bottom-up synthesis of finite models of helical (*n*,*m*)-single-wall carbon nanotubes, *Nat. Commun.*, 2011, **2**, 492.

41 A. Yagi, Y. Segawa and K. Itami, Synthesis and Properties of [9]Cyclo-1,4-naphthylene: A π-Extended Carbon Nanoring, *J. Am. Chem. Soc.*, 2012, **134**, 2962.

42 T. Sisto, X. Tian and R. Jasti, Synthesis of Tetraphenyl-Substituted [12]Cycloparaphenylene: Toward a Rationally Designed Ultrashort Carbon Nanotube, *J. Org. Chem.*, 2012, **77**, 5857.

43 K. Matsui, Y. Segawa, T. Namikawa, K. Kamada and K. Itami, Synthesis and properties of all-benzene carbon nanocages: a junction unit of branched carbon nanotubes, *Chem. Sci.*, 2013, **4**, 84.

44 J. Xia, M. Golder, M. Foster, B. Wong and R. Jasti, Synthesis, Characterization, and Computational Studies of Cycloparaphenylene Dimers, *J. Am. Chem. Soc.*, 2012, **134**, 19709.

45 P. Kim, K. H. Park, W. Kim, T. Tamachi, M. Iyoda and D. Kim, Relationship between Dynamic Planarization Processes and Exciton Delocalization in Cyclic Oligothiophenes, *J. Phys. Chem. Lett.*, 2015, **6**(3), 451–456, available from: http://pubs.acs.org/doi/abs/10.1021/jz502395z.

46 M. Peña-Alvarez, L. Qiu, M. Taravillo, V. G. Baonza, M. C. R. Delgado and S. Yamago, *et al.*, From linear to cyclic oligoparaphenylenes: electronic and molecular changes traced in the vibrational Raman spectra and reformulation of the bond length alternation pattern, *Phys. Chem. Chem. Phys.*, 2016, **18**(17), 11683–11692, available from: http://xlink.rsc.org/?DOI=C5CP05500H.

47 F. Grein, Twist Angles and Rotational Energy Barriers of Biphenyl and Substituted Biphenyls, *J. Phys. Chem. A*, 2002, **106**, 3823.

48 H. Chen, M. R. Golder, F. Wang, S. K. Doorn, R. Jasti and S. Tretiak, *et al.*, Raman-active modes of even-numbered cycloparaphenylenes: comparisons between experiments and density functional theory (DFT) calculations with group theory arguments, *J. Phys. Chem. C*, 2015, **119**(5), 2879–2887.

49 L. Adamska, I. Nayyar, H. Chen, A. Swan, N. Oldani and S. Fernandez-Alberti, *et al.*, Self-trapping of excitons, violation of Condon approximation and efficient fluorescence in conjugated cycloparaphenylenes, *Nano Lett.*, 2014, **14**, 6539–6546.

50 E. R. Darzi and R. Jasti, The dynamic, size-dependent properties of [5]–[12]cycloparaphenylenes, *Chem. Soc. Rev.*, 2015, **44**(18), 6401–6410, available from: http://xlink.rsc.org/?DOI=C5CS00143A.

51 E. Darzi, T. Sisto and R. Jasti, *J. Org. Chem.*, 2012, **77**, 6624–6628.

52 T. Nishihara, Y. Segawa, K. Itami and Y. Kanemitsu, Excited states in cycloparaphenylenes: dependence of optical properties on ring length, *J. Phys. Chem. Lett.*, 2012, **3**(21), 3125–3128.

53 J. Liu, L. Adamska, S. K. Doorn and S. Tretiak, Singlet and triplet excitons and charge polarons in cycloparaphenylenes: a density functional theory study, *Phys. Chem. Chem. Phys.*, 2015, **17**, 14613–14622, available from: http://xlink.rsc.org/?DOI=C5CP01782C.

54 J. Cornil, D. Beljonne, C. Heller, I. Campbell, B. Laurich and D. Smith, *et al.*, Photoluminescence Spectra of Oligo-Paraphenyllenevinylenes: A Joint Theoretical and Experimental Characterization, *Chem. Phys. Lett.*, 1997, **278**, 139–145.

55 S. Tretiak, A. Saxena, R. L. Martin and A. R. Bishop, Conformational dynamics of photoexcited conjugated molecules, *Phys. Rev. Lett.*, 2002, 97402–97406.

56 N. Banerji, S. Cowan, E. Vauthey and A. Heeger, Ultrafast Relaxation of the Poly(3-hexylthiophene) Emission Spectrum, *J. Phys. Chem. C*, 2011, **115**, 9726–9739.

57 E. Busby, E. Carroll, E. Chinn, L. Chang, A. Moule and D. Larsen, Excited-State Self-Trapping and Ground-State Relaxation Dynamics in Poly(3-hexylthiophene) Resolved with Broadband Pump−Dump−Probe Spectroscopy, *J. Phys. Chem. Lett.*, 2011, **2**, 2764–2769.

58 S. Westenhoff, W. Beenken, A. Yartsev and N. Greenham, Conformational Disorder of Conjugated Polymers, *J. Chem. Phys.*, 2006, **125**, 154903.

59 P. Parkinson, C. Müller, N. Stingelin, M. Johnston and M. Herz, Role of Ultrafast Torsional Relaxation in the Emission from Polythiophene Aggregates, *J. Phys. Chem. Lett.*, 2010, **1**, 2788–2792.

60 J. Clark, T. Nelson, S. Tretiak, G. Cirmi and G. Lanzani, Femtosecond Torsional Relaxation, *Nat. Phys.*, 2012, **8**, 225–231.

61 T. Nelson, S. Fernandez-Alberti, A. E. Roitberg and S. Tretiak, Nonadiabatic Excited State Molecular Dynamics: Modeling Photophysics in Organic Conjugated Materials, *Acc. Chem. Res.*, 2014, **47**, 1155–1164.

62 T. Nelson, S. Fernandez-alberti, V. Chernyak, A. E. Roitberg and S. Tretiak, Nonadiabatic Excited-State Molecular Dynamics Modeling of Photoinduced Dynamics in Conjugated Molecules, *J. Phys. Chem. B*, 2011, **115**, 5402–5414.
63 V. S. Reddy, C. Camacho, J. Xia, R. Jasti and S. Irle, Quantum dynamics simulations reveal vibronic effects on the optical properties of [*n*]cycloparaphenylenes, *J. Chem. Theory Comput.*, 2014, **10**(9), 4025–4036.
64 J. C. Tully, Molecular dynamics with electronic transitions, *J. Chem. Phys.*, 1990, **93**, 1061–1071.
65 S. Hammes-schiffer and J. C. Tully, Proton transfer in solution: Molecular dynamics with quantum transitions, *J. Chem. Phys.*, 1994, **101**(6), 4657–4667.
66 S. Tretiak and S. Mukamel, Density matrix analysis and simulation of electronic excitations in conjugated and aggregated molecules, *Chem. Rev.*, 2002, **102**(9), 3171–3212.
67 V. Chernyak, M. F. Schulz, S. Mukamel, S. Tretiak and E. V. Tsiper, Krylov-space algorithms for time-dependent Hartree-Fock and density functional computations, *J. Chem. Phys.*, 2000, **113**, 36.
68 S. Tretiak, C. M. Isborn, A. M. N. Niklasson and M. Challacombe, Representation independent algorithms for molecular response calculations in time-dependent self-consistent field theories, *J. Chem. Phys.*, 2009, **130**, 054111.
69 F. Furche and R. Ahlrichs, Adiabatic time-dependent density functional methods for excited state properties, *J. Chem. Phys.*, 2002, **117**, 7433–7448.
70 S. Tretiak and V. Chernyak, Resonant nonlinear polarizabilities in the time-dependent density functional theory, *J. Chem. Phys.*, 2003, **119**, 8809–8823.
71 M. Tommasini, V. Chernyak and S. Mukamel, Electronic density-matrix algorithm for nonadiabatic couplings in molecular dynamics simulations, *Int. J. Quantum Chem.*, 2001, **85**, 225–238.
72 V. Chernyak and S. Mukamel, Density-matrix representation of nonadiabatic couplings in time-dependent density functional (TDDFT) theories, *J. Chem. Phys.*, 2000, **8**, 3572–3579.
73 R. Send and F. Furche, First-order nonadiabatic couplings from time-dependent hybrid density functional response theory: consistent formalism, implementation, and performance, *J. Chem. Phys.*, 2010, **132**, 044107.
74 S. Mukamel, S. Tretiak, T. Wagersreiter and V. Chernyak, Electronic coherence and collective optical excitations of conjugated molecules, *Science*, 1997, **277**(5327), 781–787.
75 S. Tretiak, V. Chernyak and S. Mukamel, Recursive density-matrix-spectral-moment algorithm for molecular nonlinear polarizabilities, *J. Chem. Phys.*, 1996, **105**, 8914–8928.
76 S. Tretiak, W. M. Zhang, V. Chernyak and S. Mukamel, Excitonic couplings and electronic coherence in bridged naphthalene dimers, *Proc. Natl. Acad. Sci. U. S. A.*, 1999, **96**(23), 13003–13008.
77 M. J. S. Dewar, E. G. Zoebisch, E. F. Healy and J. J. P. Stewart, The development and use of quantum-mechanical molecular-models.76.AM1 – A new general purpose quantum-mechanical molecular-model, *J. Am. Chem. Soc.*, 1985, **107**, 3902–3909.
78 S. Tretiak, V. Chernyak and S. Mukamel, Two-dimensional real-space analysis of optical excitations in acceptor-substituted carotenoids, *J. Am. Chem. Soc.*, 1997, **119**(47), 11408–11419.
79 G. Bazan, W. Oldham, R. Lachicotte, S. Tretiak, V. Chernyak and S. Mukamel, Stilbenoid Dimers: Dissection of a Paracyclophane Chromophore, *J. Am. Chem. Soc.*, 1998, **120**, 9188–9204.
80 S. Tretiak, V. Chernyak and S. Mukamel, Excited Electronic States of Carotenoids: Time-Dependent Density-Matrix-Response Algorithm, *Int. J. Quantum Chem.*, 1998, **70**, 711–727.
81 T. Pudzich, J. Fuhrmann-lieker and R. Salbeck, Spiro Compounds for Organic Electroluminescence and Related Applications, *Adv. Polym. Sci.*, 2006, **199**, 83–142.
82 D. Ondarse-Alvarez, N. Oldani, S. Tretiak and S. Fernandez-Alberti, Computational Study of Photoexcited Dynamics in Bichromophoric Cross-Shaped Oligofluorene, *J. Phys. Chem. A*, 2014, **118**, 10742–10753.
83 N. Oldani, S. Tretiak, G. Bazan and S. Fernandez-Alberti, Modeling of Internal Conversion in Photoexcited Conjugated Molecular Donor used in Organic Photovoltaics, *Energy Environ. Sci.*, 2014, **7**, 1175–1184.
84 M a Soler, A. E. Roitberg, T. Nelson, S. Tretiak and S. Fernandez-Alberti, Analysis of state-specific vibrations coupled to the unidirectional energy transfer in conjugated dendrimers, *J. Phys. Chem. A*, 2012, **116**(40), 9802–9810, available from: http://www.ncbi.nlm.nih.gov/pubmed/22985079.
85 T. Nelson, S. Fernandez-Alberti, V. Chernyak, A. E. Roitberg and S. Tretiak, Nonadiabatic excited-state molecular dynamics: numerical tests of convergence and parameters, *J. Chem. Phys.*, 2012, **136**(5), 54108, available from: http://www.ncbi.nlm.nih.gov/pubmed/22320726.
86 S. Tretiak, V. Chernyak and S. Mukamel, Collective electronic oscillators for nonlinear optical response of conjugated molecules, *Chem. Phys. Lett.*, 1996, **259**(1–2), 55–61.
87 C. Wu, S. V. Malinin, S. Tretiak and V. Y. Chernyak, Exciton scattering and localization in branched dendrimeric structures, *Nat. Phys.*, 2006, **2**(9), 631–635.
88 R. J. Bell, P. Dean and D. C. Hibbins-Butler, Localization of normal modes in vitreous silica, germania and beryllium fluoride, *J. Phys. C: Solid State Phys.*, 1970, **3**, 2111–2118.
89 S. N. Taraskin and S. R. Elliott, Anharmonicity and localization of atomic vibrations in vitreous silica, *Phys. Rev. B: Condens. Matter Mater. Phys.*, 1999, **59**(13), 8572–8585.
90 M. Frisch, *et al.*, *Gaussian 09 Revision A.02*, 2009.
91 M. Soler, T. Nelson, A. Roitberg, S. Tretiak and S. Fernandez-Alberti, Signature of Nonadiabatic Coupling in Excited-State Vibrational Modes, *J. Phys. Chem. A*, 2014, **118**, 10372–10379, available from: http://www.ncbi.nlm.nih.gov/pubmed/24844735.
92 S. Fernandez-Alberti, A. E. Roitberg, T. Nelson and S. Tretiak, Identification of unavoided crossings in nonadiabatic photoexcited dynamics involving multiple

electronic states in polyatomic conjugated molecules, *J. Chem. Phys.*, 2012, **137**(1), 14512, available from: http://www.ncbi.nlm.nih.gov/pubmed/22779670.

93 S. Tretiak, A. Saxena, R. Martin and A. Bishop, Conformational Dynamics of Photoexcited Conjugated Molecules, *Phys. Rev. Lett.*, 2002, **89**, 97402.

94 S. Karabunarliev, M. Baumgarten, E. Bittner and K. Mullen, Rigorous Franck Condon Absorption and Emission Spectra of Conjugated Oligomers from Quantum Chemistry, *J. Chem. Phys.*, 2000, **113**, 11372–11381.

95 I. Franco and S. Tretiak, Electron-vibrational dynamics of photoexcited polyfluorenes, *J. Am. Chem. Soc.*, 2004, **126**(38), 12130–12140.

96 H. E. Zimmerman and I. V. Alabugin, Excited state energy distribution and redistribution and chemical reactivity; mechanistic and exploratory organic photochemistry, *J. Am. Chem. Soc.*, 2000, **122**(5), 952–953.

97 A. V. Aggarwal, A. Thiessen, A. Idelson, D. Kalle, D. Würsch and T. Stangl, *et al.*, Fluctuating exciton localization in giant π-conjugated spoked-wheel macrocycles, *Nat. Chem.*, 2013, **5**(11), 964–970, available from: http://www.ncbi.nlm.nih.gov/pubmed/24153376.

98 I. G. Scheblykin, Conjugated macrocycles: Excitations get random, *Nat. Chem.*, 2013, **5**(11), 903–904, available from: http://www.nature.com/doifinder/10.1038/nchem.1787.

99 J. H. Kim, A. R. T. Nugraha, L. G. Booshehri, E. H. Hároz, K. Sato and G. D. Sanders, *et al.*, Coherent phonons in carbon nanotubes and graphene, *Chem. Phys.*, 2013, **413**, 55–80, available from: http://dx.doi.org/10.1016/j.chemphys.2012.09.017.

100 Y.-S. Lim, A. R. T. Nugraha, S.-J. Cho, M.-Y. Noh, E.-J. Yoon and H. Liu, *et al.*, Ultrafast Generation of Fundamental and Multiple-Order Phonon Excitations in Highly Enriched (6,5) Single-Wall Carbon Nanotubes, *Nano Lett.*, 2014, **14**(3), 1426–1432.

101 Y.-S. Lim, K.-J. Yee, J.-H. Kim, E. H. Hároz, J. Shaver and J. Kono, *et al.*, Coherent Lattice Vibrations in Single-Walled Carbon Nanotubes, *Nano Lett.*, 2006, **6**(12), 2696–2700.

102 J. C. Tully, Nonadiabatic Molecular Dynamics, *Int. J. Quantum Chem., Symp.*, 1991, **25**, 299–309.

103 M. D. Hack, A. W. Jasper, Y. L. Volobuev, D. W. Schwenke and D. G. Truhlar, Quantum Mechanical and Quasiclassical Trajectory Surface Hopping Studies of the Electronically Nonadiabatic Predissociation of the Ã State of NaH_2, *J. Phys. Chem. A*, 1999, **103**, 6309–6326.

104 M. Fujitsuka, T. Iwamoto, E. Kayahara, S. Yamago and T. Majima, Enhancement of the quinoidal character for smaller [*n*]cycloparaphenylenes probed by Raman spectroscopy, *ChemPhysChem*, 2013, **14**, 1570.

105 L. J. Carlson and T. D. Krauss, Photophysics of Individual Single-Walled Carbon, *Acc. Chem. Res.*, 2008, **41**(2), 235–243.

